Coherence, Compressive Sensing and Random Sensor Arrays

Lawrence Carin, Dehong Liu and Bin Guo
Department of Electrical & Computer Engineering
Duke University
Durham, NC 27708-0291
{lcarin,liudh,bg25}@ece.duke.edu

Abstract

Random sensor arrays are examined from a compressive sensing (CS) perspective, particularly in terms of the coherence of CS matrices. It is demonstrated that the maximum sidelobe level of an array corresponds to the coherence of interest for CS. This understanding is employed to explicitly quantify the accuracy of array source localization, as a function of the number of sources and the noise level. The analysis demonstrates that the CS theory is applicable to arrays in vacuum as well as in the presence of a surrounding linear media; further, the presence of a surrounding media with known properties may be used to improve array performance, with this related to phase conjugation and time reversal. Several numerical results are presented to demonstrate the theory.

I. Introduction

There has been significant recent interest in exploiting sparseness in signal recovery, based on a small number of measurements. Specifically, assume one measures $\boldsymbol{y} \in \mathbb{C}^m$, and that this signal may be represented as $\boldsymbol{y} = \boldsymbol{\Phi x} + \boldsymbol{z}$, where $\boldsymbol{\Phi} \in \mathbb{C}^{m \times n}$, $\boldsymbol{x} \in \mathbb{C}^n$ and $\boldsymbol{z} \in \mathbb{C}^m$. We are interested in the case $m < n$ and in recovering $\boldsymbol{x}$ based on the noisy measurements $\boldsymbol{y}$; $\boldsymbol{z}$ represents additive noise, or model mismatch. This problem is ill-posed without further assumptions on $\boldsymbol{x}$. However, it has recently been recognized that if $\boldsymbol{x}$ is sparse and $\boldsymbol{\Phi}$ is designed appropriately, then $\boldsymbol{x}$ may be recovered accurately (*exactly* when $\boldsymbol{z} = \boldsymbol{0}$, with $\boldsymbol{0}$ an all-zero vector) [1]–[9]. These insights have spawned the new field of compressive (or "compressed") sensing (CS).

It has recently been recognized that CS is of relevance for array signal processing [10], and particularly for analysis of random arrays. The aforementioned matrix $\boldsymbol{\Phi}$ has an interesting physical interpretation for array processing: Each column of $\boldsymbol{\Phi}$ corresponds to an angle at which a far-zone source may be located, and each row of $\boldsymbol{\Phi}$ corresponds to a particular sensor on the array; the components of $\boldsymbol{x}$ represent the angle-dependent source amplitudes, with this assumed to be

a sparse vector. It was demonstrated in [10] that the type of measurements taken by an array are consistent with CS theory, in that the measurement performed by a single array element corresponds to a Green's-function-defined projection on all angle-dependent far-zone sources. Further, as a consequence of the Green's function, each such projection measurement is "spread out" across all components of $\boldsymbol{x}$, and hence each component of $\boldsymbol{y}$ contains information about all components of $\boldsymbol{x}$. Such projection-type measurements are at the heart of compressive sensing [1]–[5]; if these projection measurements are orthogonal or nearly orthogonal, one may optimize the information accrued in each component of $\boldsymbol{y}$ about all components of the unknown $\boldsymbol{x}$. It was demonstrated [10] that if the antenna elements in the array are separated by a half-wavelength or more, the desired near-orthogonal CS projections are manifested.

The connection of CS theory to array signal processing suggests forms of array construction. Specifically, it is desirable to place array elements at spacing greater than or equal to $\lambda/2$, where λ is the wavelength. The elements may be placed at random positions as long as this inter-spacing condition is met. This is of significant practical interest, because design of random arrays has been a problem of longstanding interest. The principal historical reason for developing random arrays was to increase the array aperture with a relatively small number of antennas [11], [12]. The use of random inter-element placement was motivated by the idea of mitigating array "grating lobes" that are manifested by such a sub-sampled array. Non-uniform arrays have been constituted for similar reasons in interferometric sensing [13].

While the use of non-uniform and random arrays constitutes an old problem, the prior analysis applied to this problem is unsatisfactory, from multiple standpoints. For the case of non-uniform arrays [14], there are limited general theoretical developments; each array is generally designed from "scratch" to achieve a particular design goal. The theory associated with random arrays is more developed, as a result of statistical analyses [14]. However, this theory is largely unsatisfying, in that it constitutes statistical properties of sidelobes, as averaged across many randomly constituted arrays. It does not explicitly define the performance of a given random array, based on its sidelobe level; this quantitative assessment will be an important contribution of the methods developed here.

The algorithms developed independently for CS and random arrays are very closely related, with this a non-surprising consequence of the close connection between CS and random arrays. Existing array processing algorithms, such as CLEAN [13], which were developed decades ago for random arrays, are closely related to OMP and STOMP, developed recently in the CS literature [7], [9], [15]. Similar relationships hold for the RELAX algorithm [16] widely utilized in array analysis.

A key observation about the performance of CS inversion algorithms for $\boldsymbol{x}$, based on measuring $\boldsymbol{y} = \boldsymbol{\Phi x} + \boldsymbol{z}$, involves an analysis of the *coherence* of $\boldsymbol{\Phi}$ [6]–[9]. Specifically, the coherence of the columns of $\boldsymbol{\Phi}$ places requirements on the needed sparseness of $\boldsymbol{x}$, such that $\boldsymbol{x}$ may be recovered accurately (even perfectly) based on measuring $\boldsymbol{y}$. Interestingly, these requirements on $\boldsymbol{x}$ are defined for the aforementioned algorithms like OMP, and therefore they are of direct relevance for existing widely-employed array-processing algorithms [13], [16]. These new bounds from CS allow one to place bounds on array-sensing performance as a function of the specific array construction.

The coherence of the columns of $\boldsymbol{\Phi}$ will be demonstrated here to correspond to the sidelobe level of the array under study. Hence, this ubiquitous quantity from array analysis may now be used to place explicit bounds on array-processing performance, for a given array construction. Further, we relate the coherence to the field of time-reversal and phase conjugation [17], [18]. This connection motivates new array designs that achieve reliable high-resolution sensing while retaining a relatively small number of tightly situated sensors.

The remainder of the paper is organized as follows. In Section II we review CS theory of relevance for random sensor arrays. In Section III we briefly show that measurements of the type required for CS are implemented naturally in random arrays via the medium Green's function; this is true for general array constructions and general linear, isotropic media. Section III also discusses how CS theory may be used to quantify the resolution of random sensor arrays, linking coherence to array sidelobe levels. In Section IV we examine how CS theory may be used to make quantitative statements about the performance of random sensor arrays. Conclusions and directions for future research are provided in Section V.

II. Coherence and Performance Bounds

A. Restricted orthonormality and coherence

Researchers have recently examined the ability to recover $\boldsymbol{x}$ from $\boldsymbol{y} = \boldsymbol{\Phi x} + \boldsymbol{z}$, for $\boldsymbol{y} \in \mathbb{C}^m$, $\boldsymbol{x} \in \mathbb{C}^n$, $\boldsymbol{z} \in \mathbb{C}^m$ and $\boldsymbol{\Phi} \in \mathbb{C}^{m \times n}$, under the assumption $m < n$. It is assumed that the columns of $\boldsymbol{\Phi}$ are normalized to unit ℓ_2 norm. To make the recovery of $\boldsymbol{x}$ based on $\boldsymbol{y}$ well posed, it has been assumed that $\boldsymbol{x}$ is sparse [1]–[9]. In the discussion below we principally utilize the analysis framework of Tropp [7]–[9], as it yields quantities that may be readily computed and related to physical arrays.

To recover $\boldsymbol{x}$ from $\boldsymbol{y}$, under the assumption that $\boldsymbol{x}$ is sparse, one typically addresses the convex program

$$\boldsymbol{x}_* = \min_{\boldsymbol{b}} \ \frac{1}{2}\|\boldsymbol{y} - \boldsymbol{\Phi b}\|_2^2 + \gamma \|\boldsymbol{b}\|_1 \tag{1}$$

Let Λ index a subset of columns from $\boldsymbol{\Phi}$, with the matrix $\boldsymbol{\Phi}_\Lambda$ composed of the corresponding subset of columns. The *exact recovery coefficient* is defined as

$$\mathrm{ERC}(\Lambda) \stackrel{def}{=} 1 - \max_{\omega \notin \Lambda} \|\boldsymbol{\Phi}_\Lambda^\dagger \boldsymbol{\phi}_\omega\|_1 \tag{2}$$

where $\boldsymbol{\phi}_\omega$ represents the ωth column of $\boldsymbol{\Phi}$, and $\boldsymbol{\Phi}_\Lambda^\dagger$ is the pseudo-inverse for the matrix $\boldsymbol{\Phi}_\Lambda$, composed of the columns in the indexed set Λ; $\boldsymbol{\Phi}_\Lambda^\dagger = (\boldsymbol{\Phi}_\Lambda^* \boldsymbol{\Phi}_\Lambda)^{-1} \boldsymbol{\Phi}_\Lambda^*$, where $\boldsymbol{\Phi}_\Lambda^*$ represents the conjugate transpose of $\boldsymbol{\Phi}_\Lambda$. In an ℓ_2-error sense, the best approximation to $\boldsymbol{y}$ based on the columns in $\boldsymbol{\Phi}_\Lambda$ is $\boldsymbol{a}_\Lambda = \boldsymbol{\Phi}_\Lambda \boldsymbol{\Phi}_\Lambda^\dagger \boldsymbol{y}$. As discussed further below, if $\mathrm{ERC}(\Lambda) > 0$ for all sets Λ with $|\Lambda| \leq s$, then all s-sparse $\boldsymbol{x}$ may be recovered exactly from $\boldsymbol{y}$ if $\boldsymbol{z} = \boldsymbol{0}$, if we solve for $\boldsymbol{b}$ in the limit $\gamma \rightarrow 0$ (see (1)). This result is true without requiring *a priori* knowledge of which specific set Λ is responsible for the given $\boldsymbol{y}$ under test. The algorithm also works well for $\boldsymbol{z} \neq \boldsymbol{0}$, as discussed below.

For large n and reasonable values of s, it is computationally expensive to compute the ERC condition for all sets $|\Lambda| \leq s$. To arrive at a easily computed quantity, Tropp considers the summary

parameter of the columns of $\boldsymbol{\Phi}$, termed the coherence and defined as

$$\mu_c \stackrel{def}{=} \max_{\lambda \neq \omega} |\boldsymbol{\phi}_\omega^* \boldsymbol{\phi}_\lambda| \tag{3}$$

The requirement of low coherence is closely related to the restricted orthonormality property of Candès [19].

If $|\Lambda| \leq s$ and $s\mu_c \leq \frac{1}{2}$, then the ERC condition satisfies

$$\text{ERC}(\Lambda) \geq \frac{1-(2s-1)\mu_c}{1-(s-1)\mu_c} > 0 \tag{4}$$

with this employed in Corollary 9 from [8]; this corollary will play an important role in our subsequent sensor-array analysis, and is stated as follows. Assume $s\mu_c \leq \frac{1}{2}$, and Λ defines a *linearly independent* subset of columns from $\boldsymbol{\Phi}$ with $|\Lambda| \leq s$. Suppose that $\boldsymbol{y}$ is an observed signal whose ℓ_2 best approximation $\boldsymbol{a}_\Lambda$ over Λ satisfies the condition

$$\|\boldsymbol{\Phi}^*(\boldsymbol{y} - \boldsymbol{a}_\Lambda)\|_\infty \leq \gamma \frac{1-(2s-1)\mu_c}{1-(s-1)\mu_c} \tag{5}$$

where $\|\boldsymbol{v}\|_\infty$ for vector $\boldsymbol{v} = (v_1, ..., v_n)^T$ is the maximum $|v_i|$ for $i = 1, ..., n$. Let $\boldsymbol{x}_*$ solve (1) with parameter γ; we may conclude the following [8]:

- The support of $\boldsymbol{x}_*$, defined by those components of $\boldsymbol{x}_*$ that are non-zero, is contained in Λ
- Defining $\boldsymbol{c}_\Lambda = \boldsymbol{\Phi}_\Lambda^\dagger \boldsymbol{y}$, we have $\|\boldsymbol{x}_* - \boldsymbol{c}_\Lambda\|_\infty \leq \frac{\gamma}{1-(s-1)\mu_c}$
- In particular, the support of $\boldsymbol{x}_*$ contains every index λ in Λ for which $|\boldsymbol{c}_\Lambda(\lambda)| > \gamma/[1-(s-1)\mu_c]$.
- The minimizer $\boldsymbol{x}_*$ is unique.

Examining this result further, consider the case $s\mu_c \leq 1/2$ such that $\text{ERC}(\Lambda) > 0$ for $|\Lambda| \leq s$. Assume that, for *any* subset Λ with $|\Lambda| \leq s$, the columns in $\boldsymbol{\Phi}_\Lambda$ are linearly independent. In the noise-free case ($\boldsymbol{z} = \boldsymbol{0}$), assume $\boldsymbol{y} = \boldsymbol{\Phi}_\Lambda \boldsymbol{c}_\Lambda$. In the limit $\gamma \to 0$, (1) will recover $\boldsymbol{c}_\Lambda$ *exactly*, without requiring *a priori* knowledge of the particular subset Λ. This justifies the name associated with the ERC condition. For the case of noisy data and assuming $\text{ERC}(\Lambda) > 0$, γ must be made large enough such that (5) holds, this implying that the solution to (1) is typically sparser than $\boldsymbol{a}_\Lambda$ but with support restricted to that of $\boldsymbol{c}_\Lambda$ (with the sparseness increasing as the noise level increases, because small-amplitude coefficients of the underlying signal are lost in the noise). To minimize

the required γ to satisfy (5), and hence minimize the difference between $\boldsymbol{x}_*$ and $\boldsymbol{a}_\Lambda$, we desire μ_c to be as small as possible.

We also note that for the orthogonal basis pursuits (OMP) and basis pursuits (BP) algorithms Tropp [7], [9] has shown that perfect reconstruction (for $\boldsymbol{z} = \mathbf{0}$) may be achieved if

$$s < \frac{1}{2}(\mu_c^{-1} + 1) \tag{6}$$

In this context the connection of OMP and BP to existing algorithms in the array-processing literature [13] is of interest. We will focus on (6) when predicting array performance.

B. Projection design

To design a matrix $\boldsymbol{\Phi}$ with low coherence, an interesting option is to construct the elements of $\boldsymbol{\Phi}$ as i.i.d. draws of a random variable. This concept has been widely employed in CS, based on Gaussian and Bernoulli random variables [1]–[5]. However, such constructions of $\boldsymbol{\Phi}$ are not relevant for array-processing applications. We consider an alternative construction of the rows of $\boldsymbol{\Phi}$, of direct relevance for sensor arrays.

Consider a matrix $\boldsymbol{\Sigma} \in \mathbb{R}^{n \times n}$ defined by orthonormal rows. The matrix $\boldsymbol{\Phi}$ is defined by selecting m rows of $\boldsymbol{\Sigma}$ uniformly at random [20]. There are many orthonormal bases one may consider for $\boldsymbol{\Sigma}$, but all do not perform equally well for CS. Specifically, such that each component of $\boldsymbol{y}$ extracts information about all components of $\boldsymbol{x}$, it is desirable that each row of $\boldsymbol{\Sigma}$ be "spread out" as much as possible. If the rows of $\boldsymbol{\Sigma}$ are all normalized to unit ℓ_2 norm, it is optimal to minimize the mutual coherence between $\boldsymbol{\Sigma}$ and $\mathbf{I}^{n \times n}$, where the latter is the identity matrix. The mutual coherence is therefore here $\mu = \min_{i,j} |\boldsymbol{\Sigma}(i,j)|$, and the number of required CS measurements is proportional to μ^2 [20] (and therefore it is desirable to make μ as small as possible).

The parameter μ is called the *mutual* coherence for the following reason. In general the signal of interest may not be sparse in the basis $\mathbf{I}^{n \times n}$, but rather in some orthonormal basis $\boldsymbol{\Psi} \in \mathbb{R}^{n \times n}$. The signal of interest is then $\boldsymbol{\Psi}\boldsymbol{x}$, with $\boldsymbol{x}$ sparse, and we consider the matrix $\mathbf{U} = \boldsymbol{\Sigma}\boldsymbol{\Psi}$. In this case the matrix $\boldsymbol{\Phi}$ is defined by selecting m rows of $\mathbf{U}$ uniformly at random, and μ is a measure of the mutual coherence between $\boldsymbol{\Sigma}$ and $\boldsymbol{\Psi}$. However, for the array-processing applications of interest

here, we will generally be interested in $\boldsymbol{\Psi} = \mathbf{I}^{n\times n}$, and therefore we desire the rows of $\boldsymbol{\Sigma}$ to be uniformly spread out across the projection.

C. Summary

Compressive-sensing theory demonstrates that if $\boldsymbol{\Phi}$ is designed properly, then a sparse $\boldsymbol{x}$ may be recovered exactly from $\boldsymbol{y} = \boldsymbol{\Phi x}$, even when the dimensionality of $\boldsymbol{y}$ is small relative to that of $\boldsymbol{x}$. The requirements on the level of sparseness are related to properties of $\boldsymbol{\Phi}$. Further, accurate results may be recovered for noisy data $\boldsymbol{y} = \boldsymbol{\Phi x} + \boldsymbol{z}$; specifically, for sufficiently sparse $\boldsymbol{x}$ and appropriate $\boldsymbol{\Phi}$, the large-amplitude components of $\boldsymbol{x}$ are recovered accurately, and no spurious components of $\boldsymbol{x}$ are introduced.

Two key properties of $\boldsymbol{\Phi}$ are desirable. First, the rows of $\boldsymbol{\Phi}$ should be as "spread out" as much as possible across the components of $\boldsymbol{x}$, such that each component of $\boldsymbol{y}$ captures information about all components of $\boldsymbol{x}$ (this implies that the mutual coherence parameter μ should be as small as possible). These projections should be orthogononal or nearly orthogonal, such that each component of $\boldsymbol{y}$ captures *unique* information about $\boldsymbol{x}$. A closely related property is associated with the coherence μ_c associated with the normalized columns of $\boldsymbol{\Phi}$, with smaller coherence implying that the sparseness level s may be larger, while still achieving good estimates for $\boldsymbol{x}$. In this context, the following lower bound on the coherence is of interest: $\mu_c \geq 0$ for $n \leq m$, and $\mu_c \geq \sqrt{\frac{n-m}{m(n-1)}}$ for $n > m$ [21].

The coherence parameter μ_c for a given $\boldsymbol{\Phi}$ is particularly useful, since it may be computed readily. However, the price of this simplicity is that the bounds associated with the ERC parameter are often not very tight. Specifically, a tighter bound may be achieved if one employs the *cumulative* coherence [7]–[9], [22], but the computation of this parameter is more difficult.

III. Array-Based Projections, Coherence and Array Sensitivity

A. Array projections

In [10] a detailed discussion is provided on the properties of projections manifested by sensor arrays placed within linear media. For completeness of elucidating the connection of sensor arrays to CS, we here provide a summary of the analysis in [10].

Consider a current $q(r = R, \theta = \pi/2, \varphi)$ for large R and all $\varphi \in [0, 2\pi]$; this is a ring of current at radius $r = R$, and we assume these currents are responsible for the angle-dependent fields observed on a sensor array situated in the $\theta = \pi/2$ plane. This discussion is placed in terms of electromagnetic waves, but it is equally applicable to linear acoustic waves. In the discussion that follows, for simplicity, we consider scalar currents and Green's functions; a more-complete analysis in terms of vectors may be found in [10]. A finite sensor system ($e.g.$, array) is assumed located in the vicinity of the coordinate origin $r = 0$ (with array dimensions infinitesimal relative to R). To simplify notation, the source current $q(r = R, \theta = \pi/2, \varphi)$ is henceforth represented as $q(\varphi)$, to emphasize that it is only a function of the angle φ.

The environment in which the sensor exists is arbitrary, and the characteristics of the sensor array are general, as long as the media is isotropic and linear. For simplicity we assume the antennas are point (isotropic) radiators and receivers (Figure 1), but the theory may be generalized to consider the patterns of real antennas. The electric field due to $q(\varphi)$ as observed at the ith receiver, positioned at $\boldsymbol{r}_i$, may be expressed as

$$e(\boldsymbol{r}_i) = \int_0^{2\pi} d\varphi \; g(\boldsymbol{r}_i; r = R, \theta = \pi/2, \varphi) \; q(\varphi) \tag{7}$$

Therefore, the field $e(\boldsymbol{r}_i)$ is a linear combination (projection) of the source current $q(\varphi)$ with the Green's function $g(\boldsymbol{r}_i; r = R, \theta = \pi/2, \varphi)$. Recognizing that the source current we wish to infer always exists at $r = R$ and $\theta = \pi/2$, we also simplify the representation of the Green's function, with $g(\boldsymbol{r}_i; r = R, \theta = \pi/2, \varphi)$ henceforth represented as $g(\boldsymbol{r}_i; \varphi)$.

The observed electric fields at $\boldsymbol{r}_i$ and $\boldsymbol{r}_j$ (two antennas on the array) are manifested by projecting $q(\varphi)$ onto $g(\boldsymbol{r}_i; \varphi)$ and $g(\boldsymbol{r}_j; \varphi)$, respectively. We wish to examine the relationship between these two projections. For this, let q_1 be a point source situated at $\boldsymbol{r}_i$, and let q_2 be generated by $q_{PC}(\varphi)$ for all $\varphi \in [0, 2\pi]$, where $q_{PC}(\varphi)$ represents the phase-conjugated electric fields at $r = R$ and $\theta = \pi/2$ for $0 \leq \varphi \leq 2\pi$, due to a point source at $\boldsymbol{r}_j$; stated explicitly, $q_1 = \delta(\boldsymbol{r} - \boldsymbol{r}_i)$ and $q_2 = g^*(\boldsymbol{r}_j; \varphi)$. Using reciprocity [10], [23]

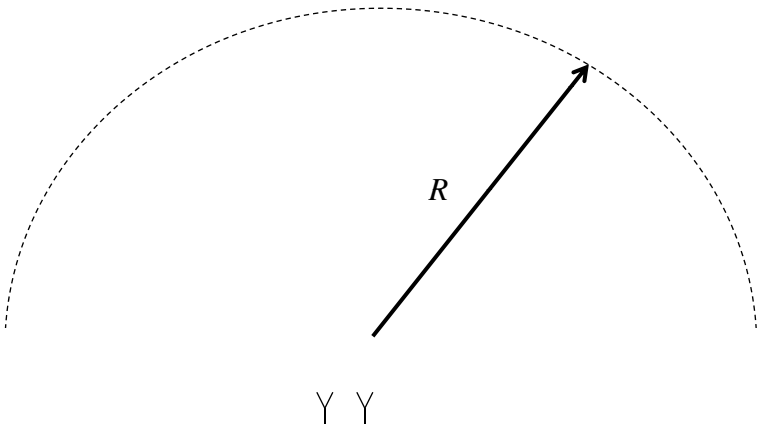

Fig. 1. Geometry of sensor array.

$$e_{PC}(\boldsymbol{r}_{obs} = \boldsymbol{r}_i; \boldsymbol{r}_{source} = \boldsymbol{r}_j) = \int_0^{2\pi} d\varphi \; g(\boldsymbol{r}_i; \varphi) g^*(\boldsymbol{r}_j; \varphi) \tag{8}$$

where $e_{PC}(\boldsymbol{r}_{obs} = \boldsymbol{r}_i; \boldsymbol{r}_{source} = \boldsymbol{r}_j)$ is the radiated field observed at $\boldsymbol{r}_i$ due to $q_2 = q_{PC}(\varphi) = g^*(\boldsymbol{r}_j; \varphi)$. Because of the fact that the current $q_{PC}(\varphi)$ resides for all $\varphi \in [0, 2\pi]$, and using insights from phase conjugation or time-reversal [17], the $e_{PC}(\boldsymbol{r}_{obs} = \boldsymbol{r}_i; \boldsymbol{r}_{source} = \boldsymbol{r}_j)$ will be strongly peaked at $\boldsymbol{r}_i = \boldsymbol{r}_j$, and will become very small for $\|\boldsymbol{r}_i - \boldsymbol{r}_j\|_{\ell_2} > \lambda/2$, where λ is the wavelength. This demonstrates that if $\|\boldsymbol{r}_i - \boldsymbol{r}_j\|_{\ell_2} \geq \lambda/2$ the projections manifested by $g(\boldsymbol{r}_i; \varphi)$ and $g(\boldsymbol{r}_j; \varphi)$ are approximately orthogonal:

$$\int_0^{2\pi} d\varphi \; g(\boldsymbol{r}_i; \varphi) g^*(\boldsymbol{r}_j; \varphi) \approx 0 \quad \text{for} \quad \|\boldsymbol{r}_i - \boldsymbol{r}_j\|_{\ell_2} \geq \lambda/2 \tag{9}$$

The $\lambda/2$ resolution is dictated by the fact that, for the large R of interest, the current $q_{PC}(\varphi)$ loses evanescent-field information about the point source at $\boldsymbol{r}_j$ [23].

We may therefore generally view, for any antenna positions, the observed fields as projections of far-field sources at $\varphi \in [0, 2\pi]$ onto the corresponding Green's function, and the projections are orthogonal over $\varphi \in [0, 2\pi]$ as long as the antennas are separated by a half wavelength or more.

Consider an array of m isotropic antennas in the plane $\theta = \pi/2$, with the antennas situated near the

origin $r = 0$. Let y_i represent the (complex) signal measured on antenna i, and $\boldsymbol{y} = [y_1, y_2, ..., y_m]^T$ represents the data observed on the m antennas. Further, let vector $\boldsymbol{j}$ represent the (unknown) radiating currents as a function of n discretized angles (with current direction consistent with the polarization of the antennas). In this representation the current is discretized at an appropriate (fine) angular rate, discussed further below, yielding an n-dimensional vector $\boldsymbol{j}$. The current represented by $\boldsymbol{j}$ is also assumed to reside in the plane $\theta = \pi/2$ of the sensor array.

In matrix form we have

$$\boldsymbol{y} = \boldsymbol{\Phi}\boldsymbol{j} \tag{10}$$

where $\boldsymbol{\Phi}$ is an $m \times n$ matrix (with $m < n$, and ideally $m \ll n$). The ith row of $\boldsymbol{\Phi}$ represents $g(\boldsymbol{r}_i; \varphi)$ discretized with respect to φ; if all antennas are separated by at least $\lambda/2$, the rows of $\boldsymbol{\Phi}$ are approximately orthogonal. The columns of $\boldsymbol{\Phi}$ correspond to the discretized angles. If there are only a relatively sparse set of angles with strong associated sources, we may represent $\boldsymbol{y} = \boldsymbol{\Phi}\boldsymbol{x} + \boldsymbol{z}$, where $\boldsymbol{x}$ corresponds to $\boldsymbol{j}$ with the small source currents set to zero ($\boldsymbol{x}$ is sparse), and $\boldsymbol{z}$ represents the noise term (accounting for components of $\boldsymbol{j}$ not contained in $\boldsymbol{x}$). Therefore, the construction is precisely in the form required of CS theory. By construction, the columns of $\boldsymbol{\Phi}$ are normalized to unit ℓ_2 norm, with normalizing constants absorbed in $\boldsymbol{j}$.

This demonstrates that if the antenna elements in an array are separated by $\lambda/2$ or more, to a very good approximation each of the projections are very nearly orthogonal, consistent with the desired properties in CS matrices [20]. However, we also desire the projections to be mutually incoherent with $\mathbf{I}^{n\times n}$. We consider the special but important case of an antenna array in vacuum (free-space). For sources at large distances R from the array, and assuming time dependence $\exp(j\omega t)$, the free-space Green's function is of the form $\exp(-j\beta R)\exp(-j\beta\rho\cos(\varphi))/R$ [23], where ρ is the small (relative to R) distance from the origin to the corresponding antenna element on the array, $\beta = 2\pi/\lambda$, φ is the angle of observation within the array plane, and here $j = \sqrt{-1}$. Note that this projection has *constant* amplitude with respect to φ, and therefore is maximally spread out in the column space of $\boldsymbol{\Psi} = \mathbf{I}^{n\times n}$. Therefore, Green's-function-constituted projections for random arrays in vacuum are *optimal* for (typical) sources of the type mentioned above, for which $\boldsymbol{\Psi} = \mathbf{I}^{n\times n}$.

B. Coherence, sidelobes and phase conjugation

Assume that the currents on the m elements of an antenna array are represented as $(q_1, \ldots, q_m)$, with the associated array elements located respectively at $(\boldsymbol{r}_1, \ldots, \boldsymbol{r}_m)$. The far-zone radiated fields at angle φ may be represented as

$$e(\varphi) = \sum_{l=1}^{m} q_l g(\boldsymbol{r}_l; \varphi) \tag{11}$$

Assume we wish to point radiation in the direction φ_i. To do this we may place a source at (R, φ_i), radiate it and measure the received signal at each of the aforementioned m elements; the respective received signals on the m point receivers are respectively $g(\boldsymbol{r}_1; \varphi_i), \ldots, g(\boldsymbol{r}_m; \varphi_i)$. Using ideas from phase conjugation and time reversal [17], [18], to point the array in the direction φ_i, the observed signals $g(\boldsymbol{r}_1; \varphi_i), \ldots, g(\boldsymbol{r}_m; \varphi_i)$ are phase conjugated and radiated from the respective antennas, yielding the φ-dependent radiated pattern

$$e(\varphi) = \sum_{l=1}^{m} g^*(\boldsymbol{r}_l; \varphi_i) g(\boldsymbol{r}_l; \varphi) \tag{12}$$

If the antenna array has sufficiently large aperture, this radiation will be strongly peaked in the direction of $\varphi = \varphi_i$.

We now recall that the vector $\boldsymbol{x} \in \mathbb{C}^n$ represents the source amplitudes at the n discrete angles used in the array analysis, and each column of $\boldsymbol{\Phi}$ corresponds to one component of $\boldsymbol{x}$ (with corresponding angle). We assume (for simplicity) that each of the possible n sources, at the n discrete angles, are polarized in the same direction (aligned with the polarization of the receiver antennas), and the m receiver-array elements are positioned at $\boldsymbol{r}_l$, $l = 1, \ldots, m$. The ith column of $\boldsymbol{\Phi}$ is represented (apart from a normalizing constant) as $\boldsymbol{\phi}_i = (g(\boldsymbol{r}_1; \varphi_i), g(\boldsymbol{r}_2; \varphi_i), \ldots, g(\boldsymbol{r}_m; \varphi_i))^T$, where $g(\boldsymbol{r}_l; \varphi_i)$ is the Green's function for a far-zone source at angle φ_i and a receiver at $\boldsymbol{r}_l$; φ_i corresponds to the center of the ith discretized angular bin, and $i = 1, \ldots, n$. The ith column of $\boldsymbol{\Phi}$ corresponds to a source at angular bin i, as observed on each of the m sensor arrays.

We may now examine $< \boldsymbol{\phi}_i, \boldsymbol{\phi}_j >$, the inner product between the ith and jth columns of $\boldsymbol{\Phi}$. Specifically

$$< \boldsymbol{\phi}_i, \boldsymbol{\phi}_j > = C \sum_{l=1}^{m} g^*(\boldsymbol{r}_l; \varphi_i) g(\boldsymbol{r}_l; \varphi_j) \tag{13}$$

which from (12) corresponds to placing currents $\boldsymbol{\phi}_i^* \in \mathbb{C}^m$ on the m elements of the array – associated with pointing the radiated beam in the direction of angle φ_i – and observing the corresponding radiated fields at angle φ_j. In (13), C is a normalizing constant (such that $< \boldsymbol{\phi}_i, \boldsymbol{\phi}_i > = < \boldsymbol{\phi}_j, \boldsymbol{\phi}_j > = 1$), with C the same for all i and j since the sources are in the array far zone. Hence, $< \boldsymbol{\phi}_i, \boldsymbol{\phi}_j >$ for $i \neq j$ corresponds to the degree an array pointed at angle φ_i "leaks" energy into angular bin φ_j. The coherence $\mu_c = \max_{i \neq j} | < \boldsymbol{\phi}_i, \boldsymbol{\phi}_j > |$ is consequently a measure of the maximum sidelobe level for the array system under study, for a prescribed set of n discrete angular bins.

The desire to reduce sidelobe levels in array systems is a problem of long-standing concern [14]. The interesting thing about this analysis is that now the maximum sidelobe level μ_c may be used to *explicitly* quantify bounds on the number of sources that may be accurately recovered with a given array system (perfect recovery in the noise-free case). Specifically, the coherence-based bounds developed by Tropp [8] and discussed in Section II-A are directly applicable. We also note that these bounds tend to be pessimistic, as discussed further when providing quantitative results.

C. Alternative array designs

One may consider design of new array concepts that *exploit* the properties of relatively complex propagation media placed in the presence of the sensor array. Specifically, to realize a large effective aperture while still maintaining a relatively small number of proximate antennas, one may place the array antennas in the presence of scatterers, as in Figure 2. This construction manifests low sidelobes $| < \boldsymbol{\phi}_i, \boldsymbol{\phi}_j > |$ for $i \neq j$ by placing a known complicated propagation media in the presence of the array, with this very closely related to ideas studied in time reversal and phase conjugation [17]. The *effective* large aperture is manifested through scattering from the media placed in the presence of the antennas; incident waves at a diversity of incident angles impinge the scatterers, and ultimately make their way to the receiver antennas. Concerning these scatterers placed in the presence of the array antennas, it is desirable that they not break out-of-plane symmetry, to preserve polarization purity in the observed fields. This suggests placing all randomly placed antennas in the same plane, with the surrounding scatterers defined by spheres, with sphere equators residing in this same plane.

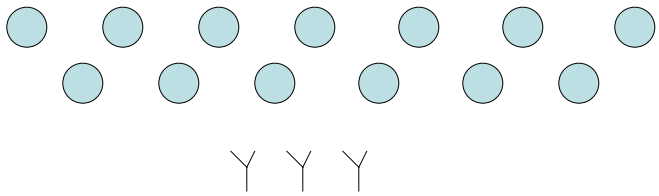

Fig. 2. Antennas in presence of scatterers.

Time reversal and phase conjugation have been understood for many years as means of exploiting complex media to enhance resolution. What is new here is that the sidelobe levels are employed within CS theory to explicitly quantify the performance of sensor arrays, for sensing angle-dependent sources. For a given array of antennas, the surrounding scatterers reduce the coherence μ_c (reduce sidelobes), and μ_c may be used to quantify bounds on improvements in array performance.

IV. Random Arrays and Source Localization

A. Random arrays in vacuum

To demonstrate the theory introduced above, we first consider a linear array situated in free space (vacuum). Specifically, we consider an array operating at 3 GHz, and our objective is to achieve the resolution of a $\lambda/2$-sampled 4 meter array, using a non-uniformly sampled array with a relatively small number of antennas. We reiterate that, while these examples consider electromagnetic waves, the results are equally applicable to linear-acoustic arrays. If the 4 meter aperture is sampled uniformly with $\lambda/2$ spacing, 81 antenna elements are required. This fully-sampled array will constitute the basis from which the non-uniform arrays are analyzed. Specifically, the n angular bins that discretize the angle-dependent far-zone sources are defined in terms of a uniformly sampled 4 meter array with $\lambda/2$ inter-element spacing.

Consider adjacent discretized angles φ_i and $\varphi_{i+1} = \varphi_i + \Delta_i$, as viewed by the $m = 81$ array elements in a $\lambda/2$-sampled uniform array distributed over 4 meters. The normalized observed signals across the m-element array, produced by a source at φ_i, are $\boldsymbol{f}_i = \frac{1}{m}(1, \exp(j\pi\cos\varphi_i), \ldots, \exp(j(m-1)\pi\cos\varphi_i))^T$, and those due to a source at $\varphi_{i+1} = \varphi_i + \Delta_i$ are $\boldsymbol{f}_{i+1} = \frac{1}{m}(1, \exp(j\pi\cos\varphi_{i+1}), \ldots, \exp(j(m-1)\pi\cos\varphi_{i+1}))^T$; again, in this context $j = \sqrt{-1}$. The inner product between these observed signals

is

$$< \boldsymbol{f}_i, \boldsymbol{f}_{i+1} >= \frac{1}{m^2} \sum_{l=1}^{m} \exp\{j(l-1)\pi[\cos(\varphi_i + \Delta_i) - \cos(\varphi_i)]\} \tag{14}$$

The Δ_i between consecutive angles, defining the discretization of the angular space, is selected such that $| < \boldsymbol{f}_i, \boldsymbol{f}_{i+1} > |$ is less than or equal to a prescribed value, defining the coherence [8], [9] of the array. For the example considered here Δ_i is selected such that a coherence of 0.15 is achieved for the uniformly filled 4 meter array with $\lambda/2$ spacing, yielding the angle bins reflected in Figure 3. Note that this yields *non-uniform* angular bins, with $\Delta = 1.26^o$ broadside to the array, and $\Delta = 5.76^o$ near grazing to the array (near 0^o and 180^o). There are a total of 91 angular bins.

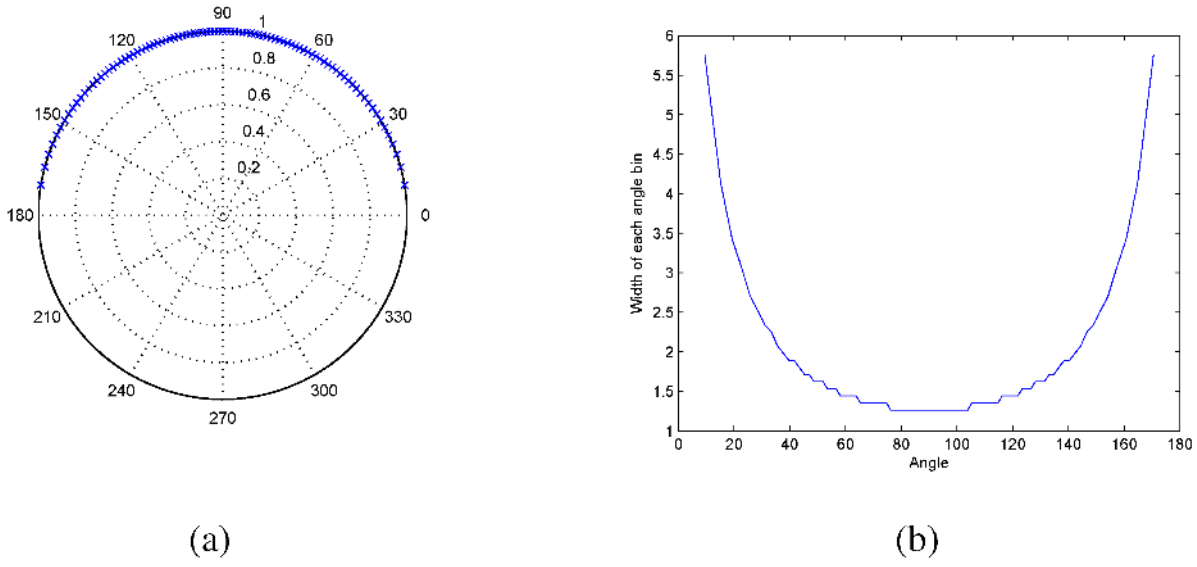

Fig. 3. Angle-bin decomposition based on an 81-element uniformly sampled array, with $\lambda/2$ inter-element spacing at 3 GHz (4 meter aperture). (a) the symbols denote the center of each angular bin; (b) angular width Δ_i of each bin, in degrees.

Using the angular bins reflected in Figure 3, we now consider arrays designed using a smaller number of antenna elements. In these examples the number of CS-type measurements corresponds to the number of antenna elements m, and the number of unknowns corresponds to the number of angular bins $n = 91$. Recall that the optimal coherence that can possibly be achieved is $\sqrt{\frac{n-m}{m(n-1)}}$. However, to approach this bound it is expected that the array aperture would have to be very wide.

In our first example (Figure 7) we consider $m = 21$, 31, 41 and 51, and in each case the antennas are employed in one of two designs. In one design the antennas are placed uniformly, with $\lambda/2$ inter-

element spacing; in this situation the four cases above correspond to respective antenna apertures of 1, 1.5, 2 and 3 meters. As a second design, we consider the same number of elements m, but situate them *randomly* over a 4 meter aperture. This latter design yields the same physical-size aperture as the original $\lambda/2$-spaced $m = 81$ element array considered above, but now with fewer elements. The coherences μ_c manifested by these two designs are tabulated in Table I. For the random arrays, many random draws were considered and that with the lowest coherence was selected for a given m, but the designs were otherwise not optimized.

Note that for the 4 meter array, we also considered uniform inter-element spacing, for $m = 21$, 31, 41 and 51 antennas. However, since the elements were space *uniformly* with greater-than $\lambda/2$ spacing, sidelobe levels were very high and therefore the coherence was poor. For example, for $m = 21$ the coherence was $\mu_c = 0.989$, which is even worse than the case of $m = 21$ with a 1 meter aperture and $\lambda/2$ spacing (see Table I). We therefore show no results for uniform inter-element spacing greater than $\lambda/2$, although experiments confirmed that these arrays performed very poorly. It is interesting to note that historically [14] random arrays were constituted with the goal of mitigating the aforementioned sidelobes. By contrast, the random array is manifested as a natural consequence of random CS sampling, with the maximum sidelobe level now defining the CS coherence parameter μ_c.

TABLE I

COHERENCE FOR TWO ARRAY DESIGNS, AS A FUNCTION OF THE NUMBER OF ANTENNAS m. IN ONE DESIGN THE ANTENNAS ARE PLACED UNIFORMLY, WITH $\lambda/2$ INTER-ELEMENT SPACING, AND IN THE SECOND CASE THE ANTENNAS ARE PLACED RANDOMLY OVER A 4 METER APERTURE.

	$m = 21$	$m = 31$	$m = 41$	$m = 51$
$\lambda/2$ Spacing	0.915	0.820	0.698	0.558
Random Spacing	0.326	0.296	0.264	0.248

Since all of the random designs have a coherence $\mu_c < 1/3$, it is expected based on (6) that each of these arrays should yield perfect performance in the noise-free case when up to two sources are considered from any of the $n = 91$ angular bins. By contrast, $\mu_c > 1/3$ for all of the uniform arrays with $\lambda/2$ spacing, and hence in this case (6) provides theoretical guarantees only for $s = 1$

source. Although (6) is a BP/OMP bound [7]–[9], all computations were performed using Lasso [24], which corresponds to the ℓ_1 construction in (1).

In these experiments, $s \geq 1$ sources are selected as being generated from the $n = 91$ source angles, with the particular s bins selected uniformly at random. The complex amplitude of the selected sources are also defined randomly, with the real and imaginary parts of the amplitudes drawn i.i.d. from $\mathcal{N}(0, 1)$. In these experiments, "perfect" reconstruction is defined by selecting all of the s angular bins correctly, with no sources at spurious angles, and achieving a relative ℓ_2 reconstruction error of 10^{-4} or better. Note that the Lasso algorithm must infer the proper number of sources, with this not set. The data are generated randomly in this manner 100,000 times, and based on applying Lasso to these data we quantify the probability of perfect estimation of the underlying $\boldsymbol{x}$, as defined above.

Empirical results are depicted in Figure 7. Results are not shown for the uniform array with $m = 21$ antennas (uniform $\lambda/2$ spacing, 1 meter aperture), since in that case the Lasso algorithm failed for all s considered, even for $s = 1$. We emphasize that this is largely due to the fact the the $n = 91$ angular bins were defined based on a 4 meter aperture, and therefore the 1 meter aperture simply does not have enough angular resolution. However, the results of the 1 meter array are not as bad as these results may reflect, since the definition of success is that the reconstruction is essentially perfect. However, for the 1 meter uniform array, when failure occurs, it is manifested by inferring an adjoining angular bin from that corresponding to truth. Hence, while it "fails", it does estimate the general location of the source angle, but not with high resolution. This of course motivates using a larger array, with random inter-element spacing [14].

For the case of $m = 31$, 41 and 51 and $\lambda/2$ inter-element spacing, the empirical performance reflected in Figure 7 is in good agreement with (6). Specifically, since $1/3 < \mu_c < 1$ we expect perfect recovery of $\boldsymbol{x}$ for $s = 1$, but not for $s > 1$, and this is observed in Figure 7 (top figure). For the non-uninform elements spaced over 4 meters (bottom in Figure 7) we expect perfect performance for $s \leq 2$ sources, since $1/5 < \mu_c < 1/3$ for $m = 21$, 31, 41 and 51 (see Table I). Note that, despite the fact that $\mu_c > 1/5$, all the non-unform arrays perform well for $s = 3$ sources, and for the

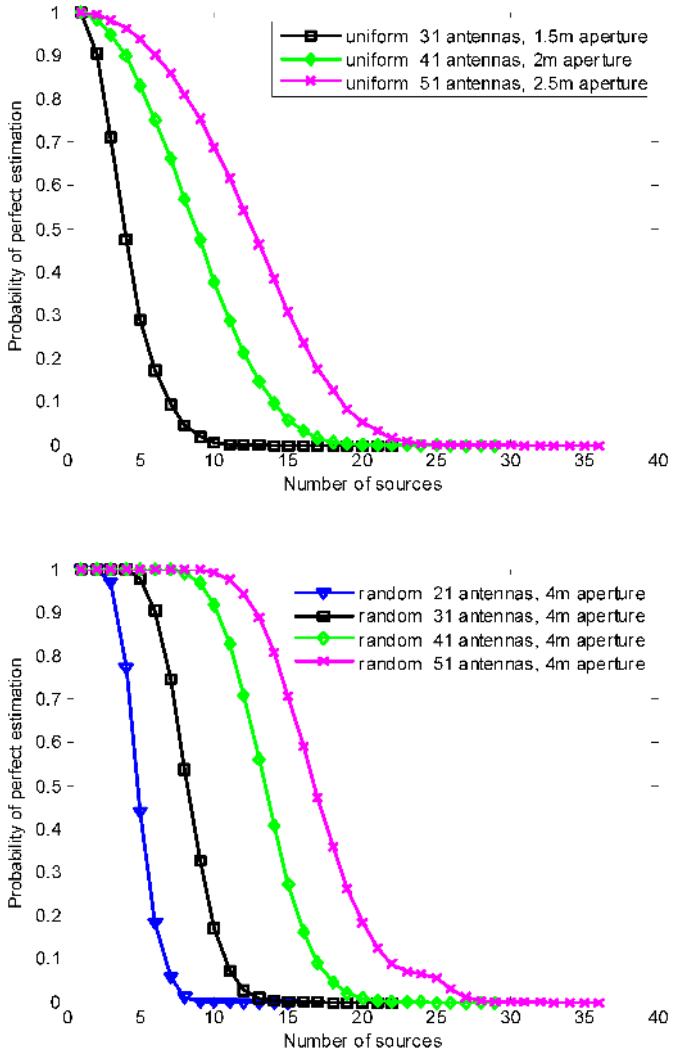

Fig. 4. Based on 100,000 runs, the probability that Lasso [24] successfully inferred the correct underlying sparse signal $\boldsymbol{x}$, as a function of the number of non-zero components s in $\boldsymbol{x}$. Success is deemed to occur if the relative ℓ_2 error between the estimated $\boldsymbol{x}_*$ and true $\boldsymbol{x}$ is less than 10^{-4}. Top: antennas placed uniformly, with $\lambda/2$ inter-element spacing, bottom: antennas placed randomly over 4 meter aperture.

$m = 51$ case $s = 10$ sources are recovered perfectly. Similar phenomenon was observed in [6], in which empirical performance was found to be better than expected based only on the coherence μ_c. This may be expected from the discussion in [7]–[9], which suggested that the coherence, while a very convenient parameter, may in some cases not yield a very tight bound. From our experiments, for a fixed (relatively large) array aperture, the bound in (6) is relatively tight for small m (short and very wide CS matrix $\boldsymbol{\Phi}$), but as m increases (more symmetric sizes of m and n in $\boldsymbol{\Phi}$, but still with $m < n$) the empirical performance is often significantly better than the bound.

We now consider noisy data $\boldsymbol{y} = \boldsymbol{\Phi x} + \boldsymbol{z}$, where $\boldsymbol{z}$ corresponds to additive complex i.i.d. Gaussian noise. We consider a 30 dB noise level, defined as $20 \cdot \log_{10}(\|\boldsymbol{\Phi x}\|_2/\|\boldsymbol{z}\|_{\ell_2})$. Results are shown in Figure 5, where we quantify the fraction of times that the estimate $\boldsymbol{x}_*$ has relative error $\|\boldsymbol{\Phi}(\boldsymbol{x}_* - \boldsymbol{x})\|_{\ell_2}/\|\boldsymbol{\Phi x}\|_{\ell_2} \leq 0.05$ (5% error), with results shown as a function of the number of sources s. In these results we again consider 100,000 realizations, with estimates $\boldsymbol{x}_*$ computed via Lasso. The random designs over a 4 meter aperture significantly outperform their uniform $\lambda/2$-spaced counterparts.

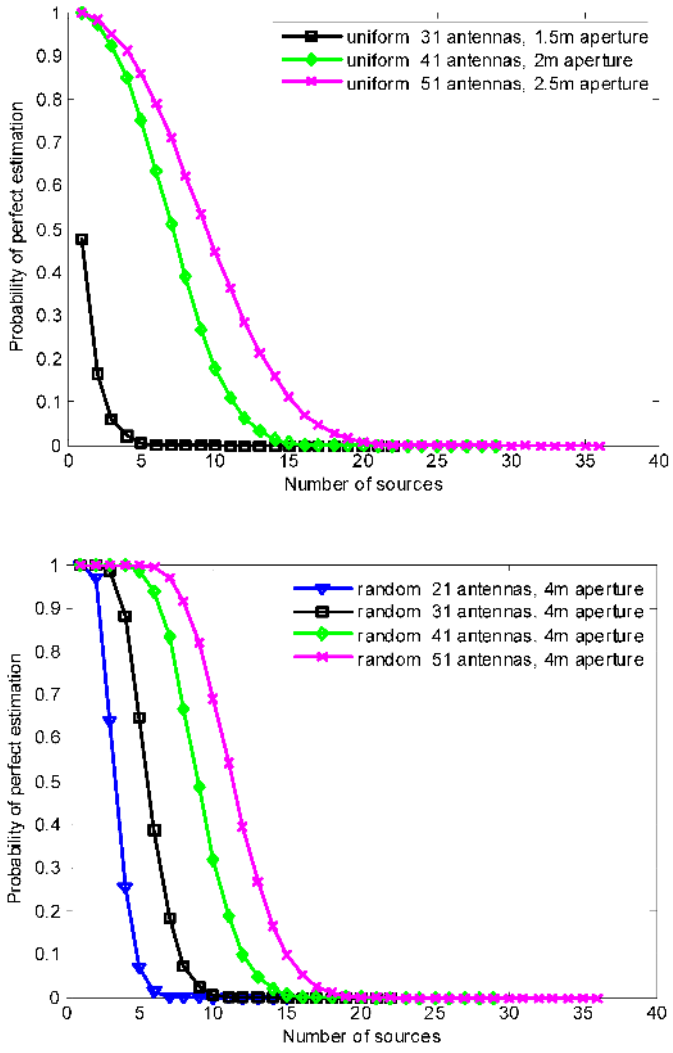

Fig. 5. Results for noisy data $\boldsymbol{y} = \boldsymbol{\Phi x} + \boldsymbol{z}$, based on 100,000 runs, considering 30 dB SNR. As a function of the number of sources s, we compute the probability that Lasso [24] yields a fraction error $\|\boldsymbol{\Phi}(\boldsymbol{x}_* - \boldsymbol{x})|_{\ell_2}/\|\boldsymbol{\Phi x}\|_{\ell_2} \leq 0.05$ (5% error). Top: antennas placed uniformly, with $\lambda/2$ inter-element spacing, bottom: antennas placed randomly over 4 meter aperture.

The results in Figures 7 and 5 suggest that, given a budget on the allowed number of antennas m that may be deployed, it appears propitious to constitute as large an aperture as physically possible, with non-uniform inter-element spacing. This empirical observation is of course supported by the theory in Sections II and III.

B. Arrays in presence of scattering media

We now consider the antenna array placed within the presence of scatterers, as in Figure 6, with the antennas in the presence of 19 perfectly reflecting spheres of radius 10 cm. The reflecting balls were placed in the presence of 21 antennas with $\lambda/2$ inter-element spacing, constituting a uniform array of 1 meter aperture (again, 3 GHz operation). The spherical balls were arranged as to constitute an approximate 4 meter aperture, in that fields incident upon the balls over a 4 meter extent will scatter to the receiver antennas (see the discussion in Section III-C). The equators of all spheres reside in a plane that bisects the $m = 21$ planar antennas. Therefore, this design is identical to the the uniformly sampled 1 meter array above, with the introduction of the spheres to manifest reduced coherence and hence increased resolution; for this geometry the coherence is $\mu_c = 0.662$.

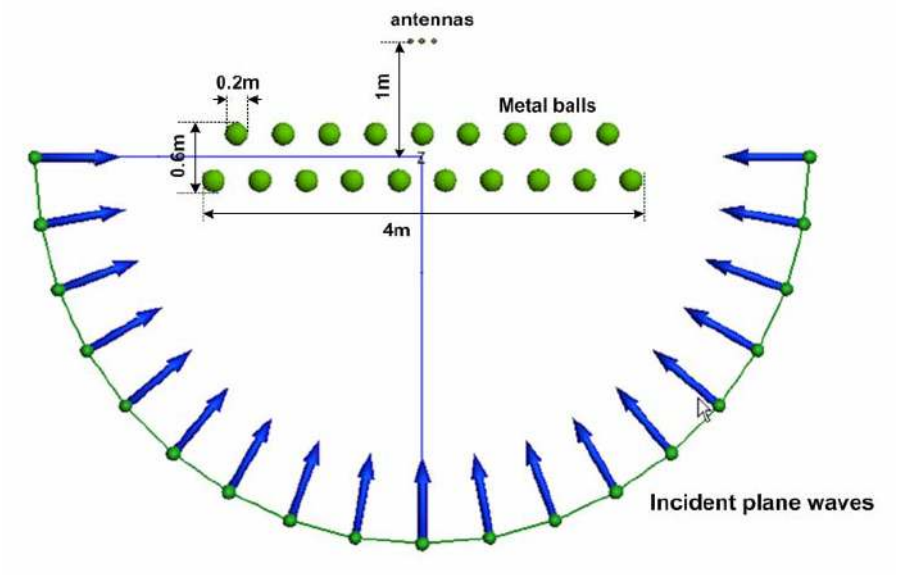

Fig. 6. Geometry of 19 perfectly conducting spheres placed in the presence of a 21-element 1 meter array, with $\lambda/2$ inter-element spacing.

To perform this analysis, we consider plane-wave incidence, and for each such plane wave the angle of incidence is at the center of one of the aforementioned $n = 91$ angular bins. When

considering $s > 1$ sources, the total signal is a superposition of s plane waves (s angles selected randomly), with complex amplitudes constituted randomly as above. To compute the plane-wave-dependent fields observed on the antennas, we employed the rigorous fast-multipole method [25].

Note that the spheres are arranged in the plane of the antennas, but there will likely be out-of-plane sources. The scatterers are constituted as spheres with the goal of preserving polarization purity. To examine this, while the equators of the spheres are in the $\theta = 90^o$ plane, in the analysis we consider vertically polarized radiation incident in the $\theta = 45^o$ plane (with discretized angles of incidence in the φ plane). The antennas are polarized as to receive vertically polarized radiation. Such designs are deemed important for practical problems, for which out-of-plane sources may be likely, and the polarization may not be known (here we measure vertically polarized components, with similar constructions possible for horizontally polarized radiation).

We consider the case of $m = 21$, with two designs: (i) antennas placed uniformly with $\lambda/2$ spacing, with the antennas placed in the presence of the 19 spherical scatterers (Figure 6); and (ii) antennas placed at random within a 4 meter aperture (with coherence μ_c in Table I), with the antennas in vacuum. Despite the fact that for this design $\mu_c > 1/3$ for case (i), as shown in Figure 7 the two designs perform almost identically. As discussed above, the uniform 1 meter aperture failed for all s when in vacuum, while if it is placed in the presence of scatterers it performs almost identical to the random 4 meter aperture in vacuum.

We also considered results of this type for noisy measurements $\boldsymbol{y} = \boldsymbol{\Phi x} + \boldsymbol{z}$, similar to those addressed in Figure 5. The noise performance of the $m = 21$ element array in the presence of the scatterers was comparable to that of the $m = 21$ element array situated randomly over 4 meters. Further details on those results are omitted here, for brevity.

V. Conclusions

Random sensor arrays have been examined from a compressive sensing (CS) perspective [1]–[9]. It has been demonstrated that sensor-array measurements are naturally in the form of CS measurements, with the CS projection-based measurements performed as a function of angle. A key parameter in quantifying the performance of such measurements is the coherence [6]–[9] of the

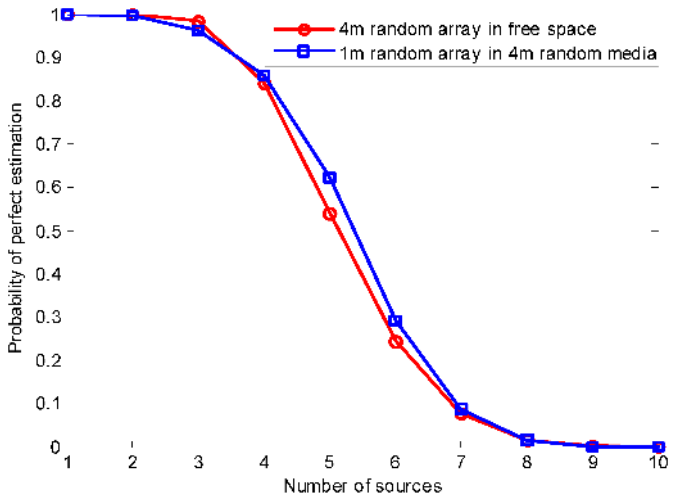

Fig. 7. Probability of successfully recovering $\boldsymbol{x}$ as a function of s, based on 100,000 randomly constituted realizations. Two $m = 21$ element array designs are considered: (i) placed in the presence of 19 spherical scatterers (Figure 6), with uniform $\lambda/2$ inter-element spacing (1 meter physical aperture); (ii) the arrays placed in vacuum, spaced at random over a 4 meter aperture. Success is deemed to occur if the relative ℓ_2 error between the estimated $\boldsymbol{x}_*$ and true $\boldsymbol{x}$ is less than 10^{-4}.

columns of the CS measurement matrix. A contribution of this paper is the demonstration that the CS coherence parameter is proportional to the maximum sidelobe level in arrays. Antenna sidelobe levels are widely employed in array analysis [14]. However, having made the connection between the maximum sidelobe level and the coherence, one may now explicitly quantify anticipated array performance in terms of relatively simple CS performance bounds [6]–[9].

Computational experiments were performed to examine the performance of random arrays, and to compare that performance to the predictions of CS theory. It was demonstrated that the performance of linear arrays is well aligned with theory, with coherence providing an important prediction of quality. The CS bounds were found to be tightest when the number of antennas m is small (short and wide CS matrix $\boldsymbol{\Phi} \in \mathbb{R}^{m \times n}$), while when the number of antennas m increases the CS theory is overly pessimistic (the bound is not tight). Related phenomenon was observed in [6].

An important aspect of most existing CS theory is that the underlying sparse signal $\boldsymbol{x}$ is assumed to be discrete. This required us to bin the angle of arrival for the far-zone sources. The size of the bins was related to the resolution of the antenna aperture, and in this sense such discretization is reasonable. Nevertheless, in reality the sources are a continuous function of angle φ, and the

concept of sparsity must be extended to a continuous signal (a continuous φ-dependent source). This corresponds to performing CS measurements for analog signals. There has been early work in this direction [26], but not directly applied to array signal processing. This is an area of future research interest.

We have also made the connection between the CS coherence parameter and phase conjugation [17], [18]. This has suggested reducing the coherence of a given antenna array by placing it in the presence of a surrounding media, with this idea demonstrated based on numerical analysis. This concept is related to the widely employed idea of employing lenses to enhance antenna performance [23]. However, such lenses are typically made out of uniform dielectric materials. Time-reversal and phase-conjugation theory suggests using more-complex scattering material to enhance performance. In the experiments considered here we have considered employing a scattering material, which suggests building future antenna lenses in terms of new metamaterials [27], that also exploit wave-scattering phenomenon. The examination of metamaterial-based antenna lenses, and placing such in the context of CS theory, is an interesting research direction.

REFERENCES

[1] E. Candès, J. Romberg, and T. Tao, "Robust uncertainty principles: Exact signal reconstruction from highly incomplete frequency information," *IEEE Trans. on Inform. Theory*, vol. 52, pp. 489–502, 2006.

[2] E. Candès and T. Tao, "Near-optimal signal recovery from random projections and universal encoding strategies," *IEEE Trans. on Inform. Theory*, vol. 52, pp. 5402–5425, 2006.

[3] E. Candès, J. Romberg, and T. Tao, "Signal recovery from incomplete and inaccurate measurements," *Communications on Pure and Applied Mathematics*, vol. 59, pp. 1207–1223, 2005.

[4] E. Candès and T. Tao, "Decoding by linear programming," *IEEE Trans. on Inform. Theory*, vol. 51, pp. 4203–4215, 2005.

[5] D. L. Donoho, "Compressed sensing," *IEEE Trans. Information Theory*, vol. 52, no. 4, pp. 1289–1306, April 2006.

[6] A. Bruckstein, D. Donoho, and M. Elad, "From sparse solutions of systems of equations to sparse modeling of signals and images," *SIAM Review*, vol. 51, pp. 34–81, March 2009.

[7] J. A. Tropp, "Greed is good: algorithmic results for sparse approximation," *Information Theory, IEEE Transactions on*, vol. 50, no. 10, pp. 2231–2242, 2004.

[8] ——, "Just relax: Convex programming methods for identifying sparse signals in noise," *IEEE Transactions on Information Theory*, vol. 52, no. 3, pp. 1030–1051, March 2006.

[9] J. A. Tropp and A. C. Gilbert, "Signal recovery from partial information via orthogonal matching pursuit," 2005.

[10] L. Carin, "On the relationship between compressive sensing and random sensor arrays," *IEEE Antennas and Propagation Magazine*, October 2009.

[11] Y. Lo, "A probabalistic approach to the problem of large antenna arrays," *Radio Science*, vol. 68D, pp. 1011–1019, 1964.

[12] ——, "A mathematical theory of antenna arrays with randomly spaced elements," *IEEE Trans. Antennas and Propagation*, vol. 12, p. 257268, 1964.

[13] J. Hogbom, "Aperture synthesis with a nonregular distribution of interferometer baselines," *Astron. Astrophys. Supplements*, vol. 15, pp. 417–426, 1974.

[14] B. Steinberg, *Principles of Aperture and Array System Design Including Random and Adaptive Arrays*. Wiley Press, 1976.

[15] D. L. Donoho, Y. Tsaig, I. Drori, and J.-C. Starck, "Sparse solution of underdetermined linear equations by stagewise orthogonal matching pursuit," 2006.

[16] J. Li and P. Stoica, "Efficient mixed-spectrum estimation with applications to target feature extraction," *IEEE Trans. Signal Processing*, vol. 44, pp. 281–295, 1996.

[17] P. Blomberg, G. Papanicolaou, and H. Zhao, "Super-resolution in time-reversal acoustics," *J. Acoust. Soc. of Am.*, vol. 111, pp. 230–248, 2002.

[18] D. Liu, G. Kang, L. Li, Y. Chen, S. Vasudevan, W. Joines, Q. H. Liu, J. Krolik, and L. Carin, "Electromagnetic time-reversal imaging of a target in a cluttered environment," *IEEE Trans. Antennas and Propagation*, vol. 53, no. 9, pp. 3058–3066, Sept. 2005.

[19] E. J. Candès, "The restricted isometry propert and its implications for compressed sensing," *Academic des Sciences*, 2008.

[20] E. Candès and J. Romberg, "Sparsity and incoherence in compressive sampling," *Inverse Problems*, vol. 23, no. 3, pp. 969–985, 2007.

[21] T. Strohmer and R. Heath, "Grassmannian frames with apoplications to coding and communication," *Appl. Comp. Harmonic Anal.*, vol. 14, no. 3, pp. 257–275, May 2003.

[22] D. Donoho and M. Elad, "Maximal sparsity representation via ℓ_1 minimization," *Proc. Nat. Acad. Sci.*, vol. 100, pp. 2197–2202, March 2003.

[23] C. Balanis, *Advanced Engineering Electromagnetics*. Wiley Press, 1989.

[24] R. Tibshirani, "Regression shrinkage and selection via the lasso," *J. Royal. Statist. Soc B.*, vol. 58, no. 1, pp. 267–288, 1996.

[25] L. Li and L. Carin, "Multilevel fast multipole calibration of ray models with application to wireless propagation," *IEEE Transactions on Antennas and Propagation*, vol. 52, pp. 2794–2800, 2004.

[26] M. Mishali and Y. Eldar, "Blind multiband signal reconstruction: compressed sensing for analog signals," *IEEE Transactions on Signal Processing*, vol. 57, no. 3, pp. 993–1009, 2009.

[27] Q. Cheng, R. Liu, J. Mock, T. Cui, and D. Smith, "Partial focusing by indefinite complementary metamaterials," *Physical Review B*, vol. 78, p. 121102, 2008.